Journal of Molecular Structure 1235 (2021) 130155

Contents lists available at ScienceDirect

Journal of Molecular Structure

journal homepage: www.elsevier.com/locate/molstr

An iron(II) complex of *trans, trans, trans-bis*(azido)*bis*(4-amino-3,5-bis(2-pyridyl)-1,2,4-triazole): Insight into molecular and supramolecular structures using Hirshfeld surface analysis and DFT studies

Zouaoui Setifi[a,b], Fatima Setifi[a,*], Christopher Glidewell[c], Diego M. Gil[d], Alexey V. Kletskov[e], Jorge Echeverria[f,*], Masoud Mirzaei[g,*]

[a] *Laboratoire de Chimie, Ingénierie Moléculaire et Nanostructures (LCIMN), Université Ferhat Abbas Sétif 1, Sétif 19000, Algeria*
[b] *Département de Technologie, Faculté de Technologie, Université 20 Août 1955-Skikda, Skikda 21000, Algeria*
[c] *School of Chemistry, University of St Andrews, St Andrews, Fife, KY16 9ST, UK*
[d] *INBIOFAL (CONICET – UNT), Instituto de Química Orgánica, Facultad de Bioquímica, Química y Farmacia, Universidad Nacional de Tucumán, Ayacucho 471, T4000INI, San Miguel de Tucumán, Argentina*
[e] *Department of Inorganic Chemistry, Faculty of Science, Peoples' Friendship University of Russia (RUDN University), 6 Miklukho-Maklaya St., Moscow 117198, Russia*
[f] *Departament de Química Inorgànica i Orgànica and Institut de Química Teòrica i Computacional (IQTC-UB), Universitat de Barcelona, Martí i Franquès 1-11, 08028 Barcelona, Spain*
[g] *Department of Chemistry, Faculty of Science, Ferdowsi University of Mashhad, Mashhad 9177948974, Iran*

ARTICLE INFO

Article history:
Received 15 January 2021
Revised 15 February 2021
Accepted 16 February 2021
Available online 26 February 2021

Keywords:
Iron(II)
Azide
DFT
Non-covalent interactions
Hirshfeld surfaces
NBO analysis

ABSTRACT

The solvothermal synthesis and structural characterization of the new high-spin iron(II) complex *trans,trans,trans*-[bis(azido)bis(4-amino-3,5-bis(2-pyridyl)-1,2,4-triazole)iron(II)] is reported. The complex crystallizes in the triclinic space group $P\bar{1}$ with $Z = 1$, $a = 6.6648(3)$ Å, $b = 8.4012(3)$ Å, $c = 11.7970(5)$ Å, $\alpha = 85.063(2)°$, $\beta = 95.063(2)°$, $\gamma = 98.5080(10)°$. It is centrosymmetric with mutually *trans* pairs of azido, pyridyl and triazole N atoms, the Fe–N distances indicate a high-spin configuration. A combination of N–H···N hydrogen bonds and $\pi\cdots\pi$ stacking interactions generates a sheet structure in which the shortest Fe···Fe distance is 6.6648(3) Å.

Hirshfeld surface analysis has been performed for visualizing, exploring and quantifying intermolecular interactions that stabilize the crystal packing of the complex. Non-covalent interactions present in the crystal structure have also been analysed by means of computational tools. The interaction energies associated with the different interaction topologies were calculated and QTAIM and NBO analyses were applied to study the origin and nature of the attractive forces.

1. Introduction

Synthesis and study of metal complexes on the basis of heterocyclic ligands is one of the most intensively developing fields of modern inorganic chemistry. The multitude of their possible practical applications constantly stimulates further research in this domain. Metal complexes bearing various heterocyclic ligands were shown to be potent catalysts [1–3] and bioactive substances [4–6], or even precursors to the synthesis of other bioa-ctive compounds on their basis [7,8]. Among the variety of heterocyclic ligands, polyheterocyclic ligands represent especially intriguing objects for use in the synthesis of metal complexes and in-depth studies of thereof. The ligands not only significantly affect the properties of the final complexes but also allow the generation of non-trivial molecular architecture variety in the solid phase [9,10]. This, simultaneously with the use of azide ligand that might serve as a bridging ligand [11], highlights a prospective direction for the creation of new solid materials with desired properties in the course of modern directed crystal engineering.

In the course of such studies, consideration of non-covalent interactions in the solid phases of corresponding metal complexes is crucial, as they not only play a major role in the formation of solid phase architecture [12,13], but also often represent interesting objects for theoretical studies that could allow more in-depth

* Corresponding authors.
E-mail addresses: fat_setifi@yahoo.fr (F. Setifi), jorge.echeverria@qi.ub.es (J. Echeverria), mirzaeesh@um.ac.ir (M. Mirzaei).

https://doi.org/10.1016/j.molstruc.2021.130155
0022-2860/

understanding and further practical application of consistent patterns lying in the formation of various crystalline motifs [14].

In this regard, it is particularly interesting to consider the cases where the azide group acts not as a bridging ligand but as a key element in the creation of non-covalently bound supramolecular architectures, especially when the application of additional polyheterocylic ligands is involved in the formation of the latter. Thus, herein we report the synthesis and in-depth studies of high-spin iron(II) complex *trans,trans,trans*-[bis(azido)bis(4-amino-3,5-bis(2-pyridyl)-1,2,4-triazole)iron(II)] by means of single-crystal X-Ray crystallography and computational methods. The detailed study is provided below.

2. Experimental

2.1. Materials and physical measurements

All chemicals were of reagent grade quality, purchased from Sigma-Aldrich Chemical Co., and used as bought without further purification.

CAUTION! Azido compounds are potentially explosive and should be prepared and used only in small amounts and treated with utmost care.

Elemental analyses were performed with a Perkin-Elmer 2400 series II CHNS/O analyzer. FT-IR spectroscopic analyses were measured at room temperature in the range of 4000–500 cm^{-1} by using a Nicolet 5SX-FTIR spectrometer equipped with a diamond micro-ATR.

2.2. Synthesis

Compound **1** was prepared solvothermally under autogenous pressure using a mixture of $FeSO_4{\cdot}7H_2O$ (28 mg, 0.1 mmol), abpt (48 mg; 0.2 mmol) and NaN_3 (13 mg, 0.2 mmol) in H_2O/EtOH (4:1 v/v, 25 ml). The mixture was sealed in a Teflon-lined autoclave and held at 170 °C for 72 h, and then cooled to room temperature at a rate of 10 °C h^{-1} (yield: 38%). Orange plates of **1** suitable for single-crystal X-ray diffraction analysis were selected. Anal. Calcd. for $C_{24}H_{20}FeN_{18}$ (616.43 g/mol): C, 46.76; H, 3.27; N, 40.90. Found: C, 46.58; H, 3.36; N, 41.02%. Main IR bands (ATR, cm^{-1}): $\nu(N_3)$: 2038(s).

2.3. X-ray crystallography

Appropriate single crystals of **1** were chosen for an X-ray diffraction study. Crystallographic measurements were collected at 170 K using a Bruker APEXII CCD diffractometer, equipped with a graphite-monochromatised Mo *Kα* radiation (λ = 0.71073 Å). Data collections were controlled by APEX2 software [15] with cell refinement and data reduction performed using SAINT [15]. Multi-scan absorption corrections were applied using SADABS [15]. The structure was solved by direct methods using SHELXS–97 [16] and refined by full-matrix least squares on F^2 with all data, using SHELXL–2014 [16]. All H atoms were located in difference maps. The H atoms bonded to C atoms were then treated as riding atoms in geometrically-idealised position with C–H distances 0.95 Å and with $U_{iso}(H) = 1.2U_{eq}(C)$. For the H atoms bonded to atom N41, the atomic coordinates were refined with $U_{iso}(H) = 1.2U_{eq}(N)$, giving the N–H distances shown in Table 3.

Crystal data and data collection procedure are summarized in Table 1. Crystallographic structural data have been deposited at the Cambridge Crystallographic Data Center (CCDC). Enquiries for data can be direct to: Cambridge Crystallographic Data Center, 12 Union Road, Cambridge, UK, CB2 1EZ or (e-mail) deposit@ccdc.cam.ac.uk or (fax) +44 (0) 1223 336,033. Any request to the Cambridge Crystallographic Data Center for this material should quote the full literature citation and the reference number CCDC 2039994.

Table 1
Crystal data and structure refinement parameters for **1**.

Chemical formula	$C_{24}H_{20}FeN_{18}$
M_r	616.43
Crystal system, space group	Triclinic, $P\bar{1}$
Temperature (K)	170
a, *b*, *c* (Å)	6.6648 (3), 8.4012 (3), 11.7970 (5)
α, *β*, *γ* (°)	95.547 (1), 95.063 (2), 98.508 (1)
V (Å^3)	646.67 (5)
Z	1
Radiation type	Mo *Kα*
μ (mm^{-1})	0.64
Crystal size (mm)	0.31 × 0.22 × 0.11
Data collection	
Diffractometer	Bruker APEXII CCD
Absorption correction	Multi-scan (*SADABS*; Bruker, 2015)
T_{min}, T_{max}	0.787, 0.883
No. of measured, independent and observed [$I > 2\sigma(I)$] reflections	40,858, 3956, 3646
R_{int}	0.038
$(\sin\theta/\lambda)_{max}$ (Å^{-1})	0.716
Refinement	
$R[F^2 > 2\sigma(F^2)]$, $wR(F^2)$, *S*	0.034, 0.077, 1.05
No. of reflections	3956
No. of parameters	202
H-atom treatment	H atoms treated by a mixture of independent and constrained refinement
$\Delta\rho_{max}$, $\Delta\rho_{min}$ (e Å^{-3})	0.39, −0.24
CCDC number	2039994

3. Theoretical methods

3.1. Hirshfeld surface calculations

The Hirshfeld surfaces and their associated 2D fingerprint plots [17–20] were generated using *CrystalExplorer*17.5 software [21] to visualize and quantify the various non-covalent interactions that are responsible of crystal stabilization. The normalized contact distance (d_{norm}) is a symmetric function of distances to the surface from nuclei inside (d_i) and outside (d_e) the Hirshfeld surface, relative to their respective van der Waals radii. Graphical plots of the Hirshfeld surfaces mapped with d_{norm} using a red-white-blue color scale, where red indicates shorter contacts, white is used for contacts around the vdW separation and blue for longer contacts. The 3D d_{norm} surfaces were mapped over a fixed color scale of −0.075 au (red) to +0.75 au (blue). Hirshfeld surfaces of the title complex were also mapped with the shape index and curvedness properties.

3.2. Computational details

Density Functional Theory (DFT) calculations were performed with Gaussian16 [22] at the B3LYP-D3 level of theory with the TZVP basis sets for all atoms. All interaction energies were calculated according to the super-molecule approach ($\Delta E_{AB} = E_{AB} - E_A - E_B$) and corrected for the BSSE by means of the counterpoise method [23]. MEP maps were built on the 0.001Å isosurface of the electron density (B3LYP/TZV) with GaussView [24]. QTAIM analysis of the topology of the electron density was carried out on the B3LYP wavefunction with AIMAll (version 19.10.12 Professional) [25]. Natural bond orbital (NBO) analyses were performed with the NBO3.1 software [26] as implemented in Gaussian16 at the same level of theory.

4. Results and discussion

4.1. Synthesis and characterization

Complex **1** was obtained in moderate yield by reacting a mixture of $FeSO_4{\cdot}7H_2O$, abpt and NaN_3 under solvothermal conditions

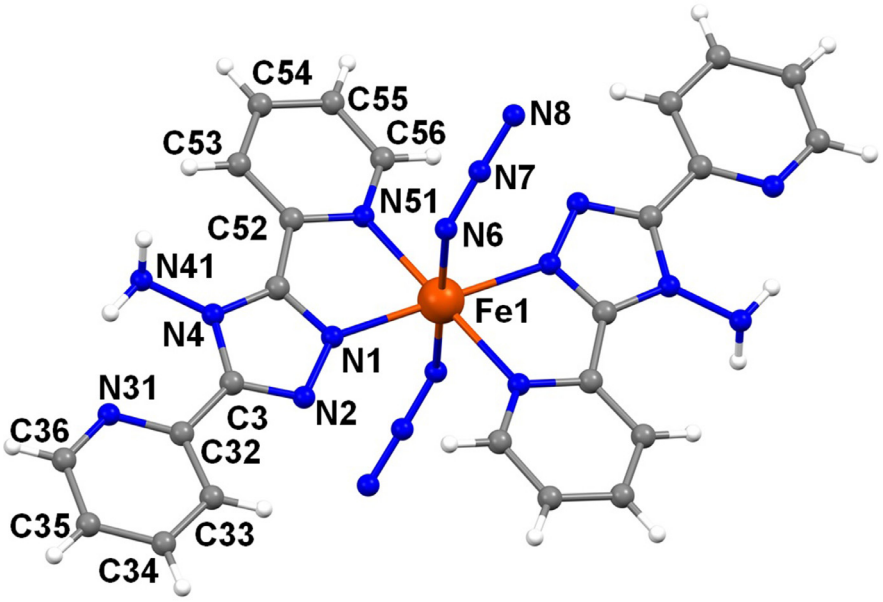

Fig. 1. The molecular structure of compound **1**, with atom labeling for the asymmetric unit. The unlabelled atoms are related to the labelled atoms by symmetry operation (1 - x, 1 - y, 1 - z).

Table 2
Selected bond lengths (Å) and angles (°) for 1.

Fe1–N1	2.1250(11)
Fe1–N6	2.1498(12)
Fe1–N51	2.2152(12)
N1–Fe1–N6	89.51(5)
N1–Fe1–N51	75.55(4)
N6–Fe1–N51	86.98(5)

in a 1:2:2 molar ratio. The identity of the title complex was proved by IR spectroscopy and elemental analysis, and the structure was also confirmed by single crystal X-ray diffraction analysis.

The IR spectrum of **1** exhibits intense absorption band centered at ca. 2038 cm^{-1}, assignable to the stretching vibration of the terminal azido ligands.

4.2. Description of the crystal structure

Compound **1** (Fig. 1) consists of two 4-amino-3,5-bis(2-pyridyl)-1,2,4-triazole ligands coordinated to iron(II) in bidentate fashion via N1 atom of the triazole unit and N51 of the 5-(2-pyridyl) unit, with the remaining two sites in the octahedral coordination being occupied by azido ligands. The complex is centrosymmetric (Table 1), with the reference unit selected as that lying across the inversion center at (0.5, 0.5, 0.5) in space group $P\bar{1}$ (Table 1). Consequently, the pairs of coordinating atoms of the azido, pyridyl and triazole units are all mutually *trans*. The triazole ring makes dihedral angles with the pyridyl rings containing N31 and N51 atoms of 4.93(1)º and 6.55(9)º, respectively, so that the non-H atoms of the organic ligand are very nearly coplanar.

The Fe–N distances (Table 2) are closely grouped in the range 2.12–2.22 Å. In general, the Fe−N distances in octahedral complexes containing pyridyl or similar ligands fall into two clearly delineated groups. In low-spin systems of this type such Fe−N distances are all closely grouped around 1.96 Å [27–33], while in high-spin systems, the Fe−N distance are all closely grouped around 2.22 Å [27,34–37]. The metrical distinction between the two groups is so clear cut as to leave little doubt that in the present complex the Fe center has a high-spin configuration, although it must be emphasized that this is based on geometry, rather than on direct measurements of magnetic susceptibility.

Table 3
Hydrogen-bond geometry (Å, º) for **1**.

D–H···A	D–H	H···A	D···A	D–H···A	Symmetry
N41–H411···N31	0.89(3)	2.086(19)	2.8444(17)	142.4(16)	x, y, z
N41-H412···N8	0.875(17)	2.108(17)	2.9774(19)	172.4(19)	1-x,2-y,1-z

In the five-membered chelate ring, the N–Fe–N angle is significantly less than 90°, as expected, but the other angles at Fe are close to 90°.

The supramolecular assembly of **1** is based upon a combination of N–H···N hydrogen bonds (Table 3) and $\pi\cdots\pi$ stacking interactions, but azido$\cdots\pi$(pyridyl) interactions are absent. One N–H···N hydrogen bond in intramolecular, utilizing the N atom of the uncoordinated pyridyl unit as the acceptor, and the other is intermolecular, with the terminal N atom of the azido ligand as acceptor. This intermolecular hydrogen bond, together with the inversion symmetry of the complex generates a *molecular ribbon running parallel to the [010] direction, with Fe atoms at (0.5, *n* + 0.5, 0.5) and $R_2^2(18)$ graph-set [38–40] centered at (0.5, n, 0.5), where n represents an integer in each case (Fig. 2). In addition, the uncoordinated pyridyl units at (x, y, z) and (-x, 1 - y, 2 - z), which are strictly parallel, have an interplanar spacing of 3.5079(6) Å, with a ring-centroid separation of 3.6678(8) Å. The combination of this interaction with the inversion symmetry generates a π-stacked chain of complexes running parallel to the [10–1] direction, in which the Fe atoms are at (*n* + 0.5, 0.5, -*n* + 0.5), where n represents an integer (Fig. 3). The combination of the chain motifs along [100] and [010] generates a complex sheet lying parallel to (101) (Fig. 4). Within the chains along [100] and [010] the shortest Fe···Fe distances are 6.6648(3) Å and 8.4012(3) Å, respectively.

4.3. Hirshfeld surface analysis

The Hirshfeld surfaces mapped over d_{norm}, shape index and curvedness properties are shown in Fig. 5. The full and decom-

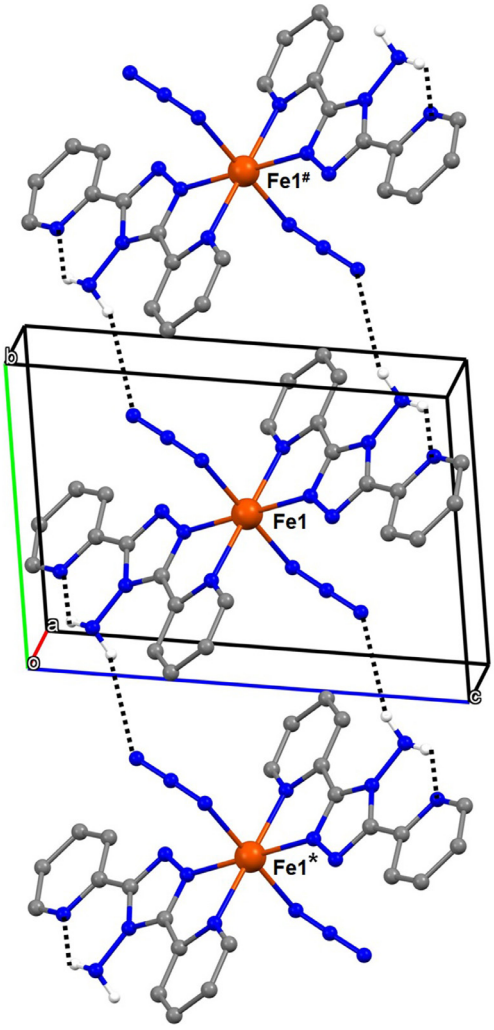

Fig. 2. Partial view of the crystal structure of **1** showing the formation of a hydrogen-bonded ribbon running parallel to the [010] direction. Hydrogen bonds are drawn as dashed lines and, for the sake of clarity, the H-atoms bonded to C atoms have been omitted. The Fe atoms marked with an asterisk (*) or a hash (#) are at (0.5, 1.5, 0.5) and (0.5, −0.5, 0.5), respectively.

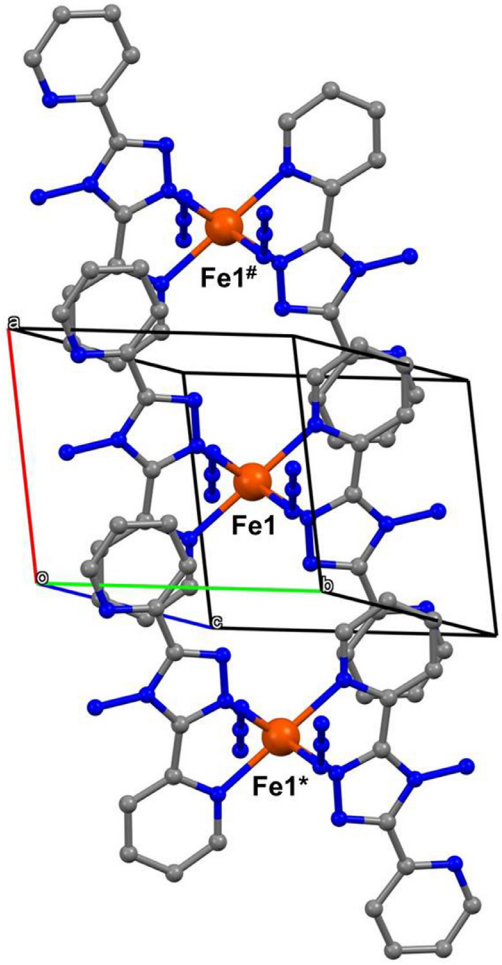

Fig. 3. Partial view of the crystal structure of **1** showing the formation of a π-stacked chain running parallel to the [10–1] direction. For the sake of clarity, the H-atoms have all been omitted, and the Fe atoms marked with an asterisk (*) or a hash (#) are at (1.5, 0.5, −0.5) and (−0.5, 0.5, 1.5), respectively.

posed 2D fingerprint plots are presented in Fig. 6. The large red regions labeled 1 in the d_{norm} surface (Fig. 5) represent H···N/N···H contacts attributed to N41−H412···N8 hydrogen bonds involving the N8 of the azido ligand as an acceptor [d(H412···N8) = 2.108 Å]. The white region located around the NH_2 group is attributed to weak N41−H411···N41 hydrogen bonds [d(H411···N41) = 2.714 Å], which is around to the sum of vdW radii of H and N-atoms. The red spots labelled 2 and 3 are attributed to C35–H35···N8 and C54−H54···N8 hydrogen bonds, respectively involving the N8 atom from the azido ligand as acceptor and the H-atoms of the pyridyl ring. These interactions are observed as symmetrical spikes at $(d_e + d_i)$ ~ 2.0 Å in the fingerprint plot (Fig. 6) with the highest contribution of 42.3% to the total Hirshfeld surface area.

The H···C/C···H contacts associated to C–H···π interactions appear as two broad spikes at $(d_e + d_i)$ ~ 2.9 Å in the fingerprint plot with 12.2% contribution to the Hirshfeld surface area. The C–H···π contacts also appear in a characteristic way in the form of pronounced “wings” on the sides of the fingerprint plots.

The red spots located in the triazole and pyridyl rings labeled 5 in the d_{norm} surface are attributed to π···π stacking interactions with an inter-centroid distance Cg···Cg of 3.8 Å. The π-stacking interactions described previously for the complex can be seen on the Hirshfeld surface mapped over shape index, as a pattern of alternating red and blue triangles highlighted as a black circle in Fig. 5. In addition, the curvedness surface clearly shows large green regions at the same side of the molecule, evidencing the presence of π···π stacking interactions. The full fingerprint plot of the complex (Fig. 6) also highlights the green region around $d_e = d_i$ = 1.8 Å, which corresponds to the π···π contacts with 9.4% of contribution to the total Hirshfeld surface area. Finally, the red areas labeled 7 in the d_{norm} surface are attributed to H34···H35 interactions with a distance of 2.260 Å, shorter than the sum of vdW radii. These H···H contacts are also visible in the middle of scattered points in the fingerprint plot with minimum $(d_e + d_i)$ contact distance of 2.0 Å, comprising a 29.8% contribution to the Hirshfeld surface area.

4.4. Computational analysis

We next undertake a computational analysis of the most relevant interactions present in the crystal structure of **1**. First, we will represent the molecular electrostatic potential (MEP) of the isolated compound **1** to try to rationalize the short contacts in terms of electrostatics. As can be seen in Fig. 7, there are two clear regions of negative electrostatic potential corresponding to the two azido ligands. In particular, the terminal nitrogen atom shows the region with the most negative value of the electrostatic

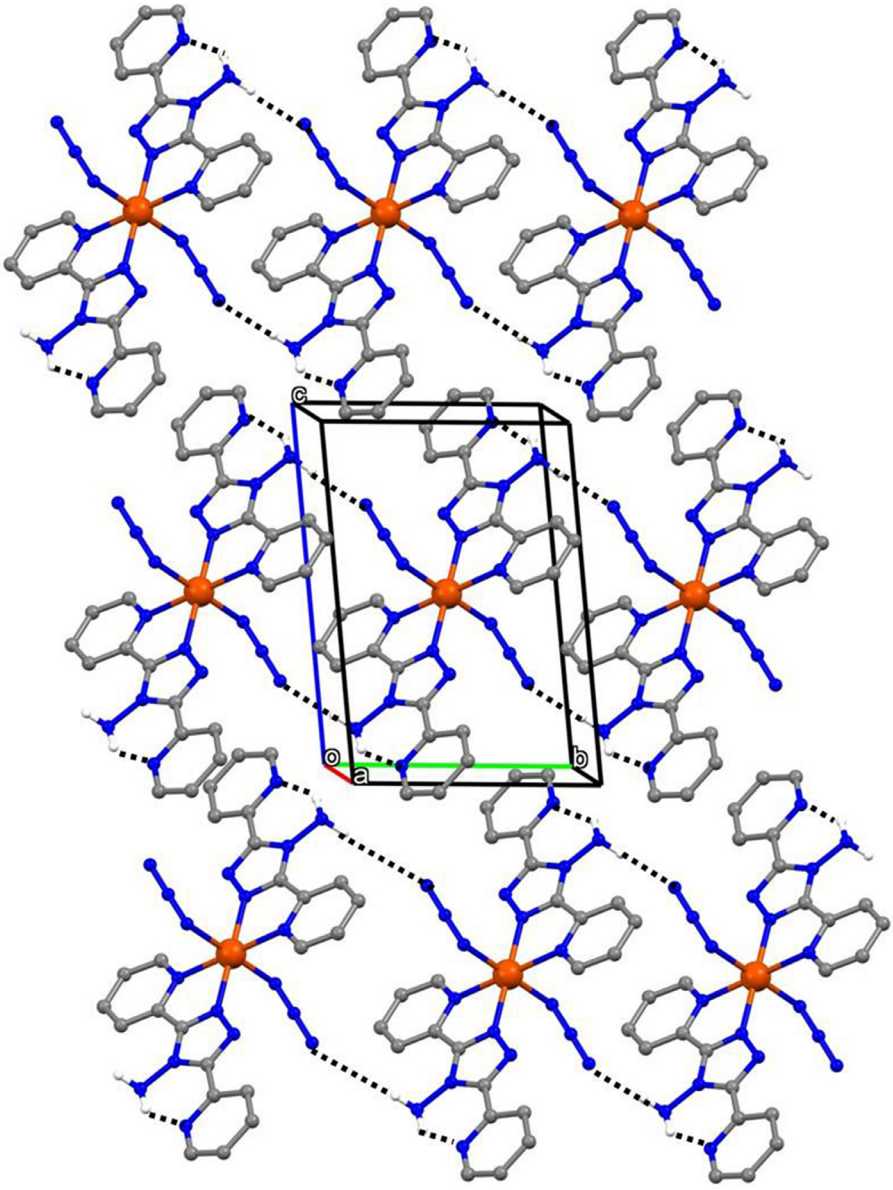

Fig. 4. Partial view of the crystal structure of **1** showing the formation of a π-stacked sheet of hydrogen-bonded ribbon lying parallel to the (101). Hydrogen bonds are drawn as dashed lines and, for the sake of clarity, the H atoms bonded to C atoms have been omitted.

potential ($V_{s,min}$ = −58.3 kcal/mol). On the other hand, the most positive regions of the electrostatic potential surface correspond to the aminic hydrogen atoms, which are out of the plane of the molecule ($V_{s,max}$ = +43.7 kcal/mol). It is precisely those two regions of depletion and accumulation of the electrostatic potential that come closer in the crystal structure to establish ~~a~~ N···H–N hydrogen bonds as shown above in Fig. 2.

For the investigation of the interaction energies and the analysis of the topology of the electron density by means of the QTAIM theory, we have separated the interacting molecules in three different dimers. On one hand we have the dimer connected via hydrogen bonds as shown in Fig. 2 (dimer **I**; see Fig. 8), and on the other hand the two dimers with the aromatic systems stacked (dimer **II** with C···C distance of 3.215 Å, and dimer **III** with C···C distance of 3.325 Å; see Fig. 9).

The calculated interaction energy for dimer **I**, with two N–H···N hydrogen bonds as the main intermolecular interactions is −28.4 kcal/mol. The QTAIM analysis shows two bond paths involving each azido ligand (Fig. 8). One corresponds to the aforementioned N–H···N_{azido} bond (**bcp1**, ρ = 0.0186 au), whereas the second one is associated with a secondary C–H···N_{azido} interaction (**bcp1**, ρ = 0.0062 au) with an interatomic distance of 2.793 Å, slightly shorter than the sum of the van der Waals radii of nitrogen and hydrogen atoms.

The interaction energies calculated for dimers **II** and **III** are −12.6 and −36.6 kcal/mol, respectively. In the case of dimer **II**, the QTAIM analysis shows three different bond paths with the corresponding bond critical points. The first one connects the two carbon atoms of the stacked pyridine rings at 3.215 Å (**bcp3**, ρ = 0.0075 au) whereas the other two are associated with C–H···N_{azido} interactions with interatomic distances of 2.660 Å (**bcp4a-b**, ρ = 0.0071 au). For dimer **III**, the QTAIM results are significantly more complex (Fig. 9). We have found 17 bond paths between the two molecules, whose main features are summarized in Table 4. From **bcp5** top **bcp12**, there are another six bcps equivalent by symmetry as can be seen in Fig. 9. On the other hand, **bcp13** corresponds to a somewhat long H···H homopolar contact (3.041 Å). However, it is worth noting that the main interaction

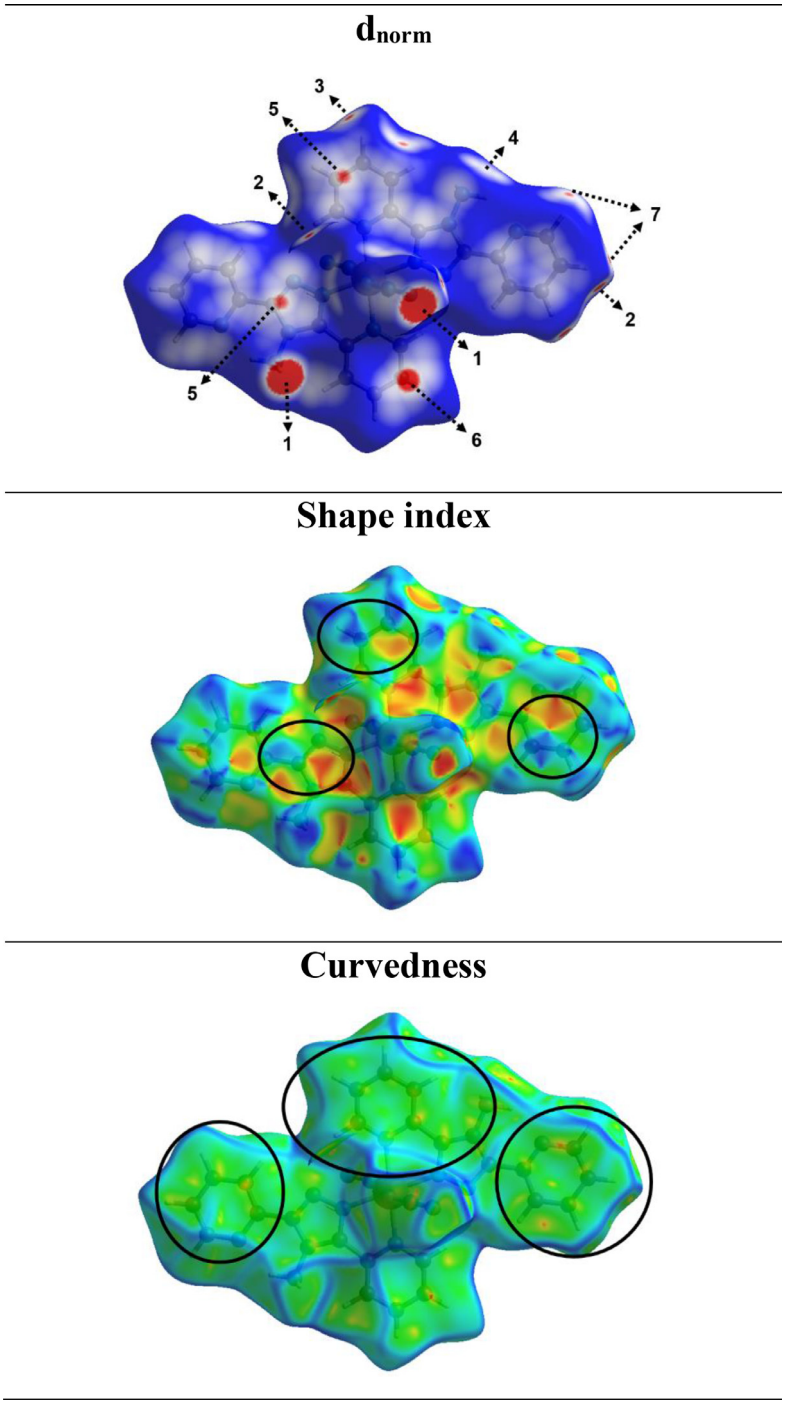

Fig. 5. Hirshfeld surfaces mapped with $d_{norm,}$ shape index and curvedness for **1**. Labels are discussed in the main text.

Table 4
Main characteristics of the bond critical points (bcp) found in the QTAIM analysis of dimer **III**.

Bcp	Interaction	dist. (Å)	ρ_{bcp}	$\nabla^2\rho_{bcp}$
5	$H_2N\cdots C_{ar}$	3.450	0.0046	0.0147
6	$N_{azido}\cdots H{-}C_{ar}$	2.870	0.0049	0.0163
7	$C_{ar}\cdots C_{ar}$	3.440	0.0049	0.0153
8	$C_{ar}\cdots C_{ar}$	3.409	0.0053	0.0162
9	$N_{azido}\cdots H{-}C_{ar}$	2.832	0.0050	0.0197
10	$N_{azido}\cdots H{-}C_{ar}$	2.903	0.0050	0.0171
11	$N_{azido}\cdots H{-}C_{ar}$	2.917	0.0044	0.0165
12	$C_{ar}\cdots C_{ar}$	3.325	0.0064	0.0197
13	$C_{ar}{-}H\cdots H{-}C_{ar}$	3.041	0.0012	0.0054

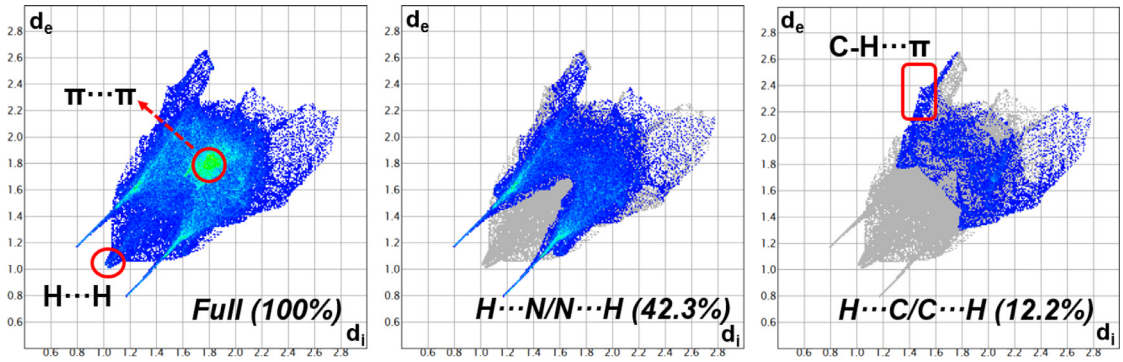

Fig. 6. Full and decomposed 2D-fingerprint plots of **1**.

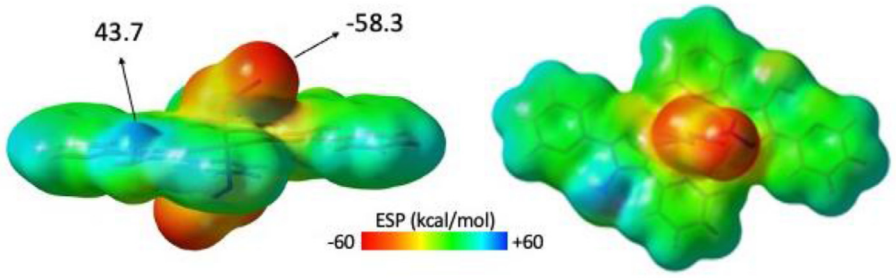

Fig. 7. Molecular electrostatic potential map of the molecular structure of compound **1** calculated at the B3LYP/TZVP level of theory. Energies are given in kcal/mol.

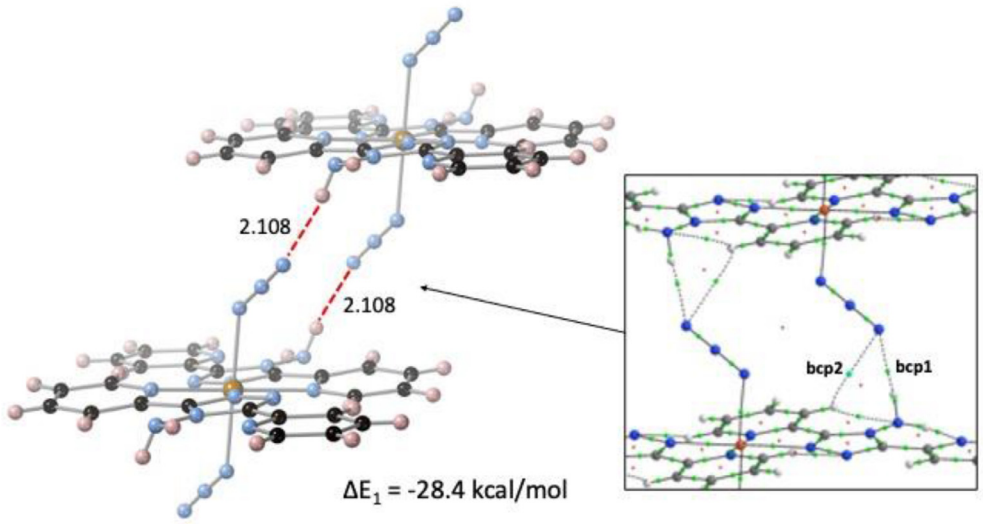

Fig. 8. Short contacts between two neighboring molecules parallel to the [010] direction (dimer **I**) and AIM results including bond paths and bond critical points. Distances are given in Å.

is associated with the shortest C···C contact at 3.325 Å (**bcp12**, $\rho = 0.0064$ au). The fact that in all cases the Laplacian of the electron density at the bcp ($\nabla^2\rho_{bcp}$) presents a positive value is characteristic of non-covalent interactions.

We have next performed a Natural Bond Orbital (NBO) analysis in order to unveil the charge transfer interactions present in dimers **I, II** and **III**. In **I**, the H-bonded dimer of Fig. 8, the only orbital interactions are between the interacting azido ligand and the N–H moiety that form the hydrogen bond. The second order perturbation energy associated with the charge transfer from the nitrogen lone pair and an empty σ antibonding of the N–H aminic bond ($LP_N \rightarrow \sigma^*_{N-H}$) accounts for 3.11 kcal/mol. There is also a secondary orbital, yet significant, mixing between an occupied π orbital of the azido and the same empty sigma antibonding of the N–H aminic bond ($\pi_{N=N} \rightarrow \sigma^*_{N-H}$) releasing 0.32 kcal/mol. In dimer **II**, the main orbital interactions from occupied to empty π orbitals are associated with the C···C short contact at 3.215 Å ($\pi_{C=C} \rightarrow \pi^*_{C=C}$ and $\pi_{C=C} \rightarrow \pi^*_{C=N}$, accounting for 0.51 and 0.08 kcal/mol, respectively). In dimer **III**, due to the presence of two stacked large aromatic systems, there are eight orbital interactions of the type $\pi_{C=C} \rightarrow \pi^*_{C=C}$, $\pi_{C=N} \rightarrow \pi^*_{C=C}$ and $\pi_{C=C} \rightarrow \pi^*_{C=N}$, with associated energies ranging from 0.10 to 0.41 kcal/mol. All these interactions (along with expected large dispersion energy), also reflected in the QTAIM analysis, contribute to the large calculated interaction energy for this dimer ($\Delta E_3 = -36.6$ kcal/mol).

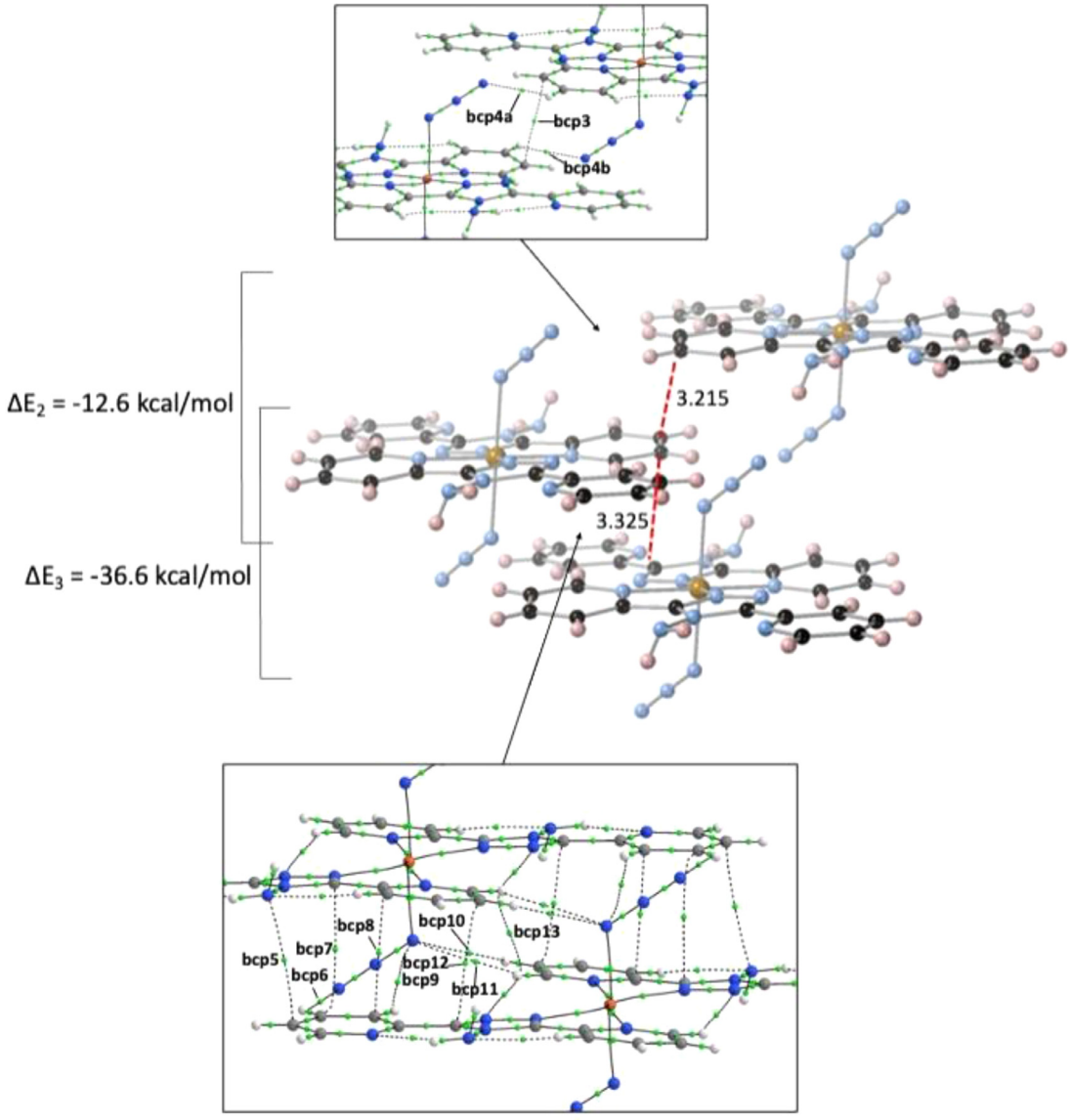

Fig. 9. Short contacts between three neighboring molecules in the π-stacked chain running parallel to the [10–1] direction (dimers **II** and **III**). Distances are given in Å.

Concluding remarks

In summary, we have synthesized and structurally characterized a new high-spin bis(azido) complex of iron(II) containing bidentate 4-amino-3,5-bis(2-pyridyl)-1,2,4-triazole ligands, and we have analysed the non-covalent intermolecular interactions using a combination of Hirshfeld surface analysis and QTAIM and NBO analyses. The complex is centrosymmetric, with an all-*trans* configuration, and the molecules are linked by a combination of hydrogen bonds and $\pi\cdots\pi$ interactions to form sheets within which the shortest Fe···Fe distance is 6.6648 (3) Å. The Hirshfeld analysis points to the importance of C–H···π contacts and $\pi\cdots\pi$ interactions in addition to the conventional N–H···N hydrogen bonds in determining the mutual arrangement of the complexes in the crystal. The computational analysis of the non-covalent interactions has disclosed the pivotal role of the azido ligand in driving the formation of the crystal structure of **1**. By means of comprehensive QTAIM and NBO analyses, we have also observed that $\pi\cdots\pi$ stacking interactions between the planar parts of the ligands are present and contribute significantly to the stabilization of systems.

Author statement

All persons listed as authors have made substantial contributions to the work reported in the manuscript (e.g., technical help, writing and editing assistance, general support).

Declaration of Competing Interest

The authors declare no conflicts of interest.

Acknowledgments

The authors thank the Algerian Ministère de l'Enseignement Supérieur et de la Recherche Scientifique (MESRS), the Direction Générale de la Recherche Scientifique et du Développement Technologique (DGRSDT) as well as the Université Ferhat Abbas Sétif 1 for financial support. J. E. is grateful to the Spanish MICCIN for a *Ramón y Cajal* research contract (RYC-2017–22853). Financial support from the Spanish Structures of Excellence María de Maeztu program (MDM-2017–0767) and Spanish MICINN through grant PID2019-109119GA-I00 are gratefully acknowledged.

Supplementary materials

Supplementary material associated with this article can be found, in the online version, at doi:10.1016/j.molstruc.2021.130155.

References

[1] M.N. Zafar, A.H. Atif, M.F. Nazar, S.H. Sumrra, R.P. Gul-E-Saba, Pyridine and related ligands in transition metal homogeneous catalysis, Russ. J. Coord. Chem. 42 (2016) 1–18, doi:10.1134/S1070328416010097.

[2] N.A. Bumagin, S.K. Petkevich, A.V. Kletskov, V.I. Potkin, 3,5-[5-arylisoxazol-3-yl(4,5-dichloroisothiazol-3-yl)]-substituted 1,2,4- and 1,3,4-oxadiazoles: synthesis, palladium complexes, and catalysis of Suzuki reactions in aqueous media, Chem. Heterocycl. Compd. 53 (2017) 1340–1349, doi:10.1007/s10593-018-2216-z.

[3] A.V. Kletskov, N.A. Bumagin, F.I. Zubkov, D.G. Grudinin, V.I. Potkin, Isothiazoles in the design and synthesis of biologically active substances and ligands for metal complexes, Synthesis (Stuttg) 52 (2020) 159–188, doi:10.1055/s-0039-1690688.

[4] D.-L. Ma, H.-Z. He, K.-H. Leung, D.S.-H. Chan, C.-H. Leung, Bioactive luminescent transition-metal complexes for biomedical applications, Angew. Chem. Int. Ed. 52 (2013) 7666–7682, doi:10.1002/anie.201208414.

[5] R. Mehrotra, S.N. Shukla, P. Gaur, A. Dubey, Identification of pharmacophore in bioactive metal complexes: synthesis, spectroscopic characterization and application, Eur. J. Med. Chem. 50 (2012) 149–153, doi:10.1016/j.ejmech.2012.01.049.

[6] L. Yang, B. Wang, J. Tan, L. Zhu, The DNA-binding and bioactivity of rare earth metal complexes, Mini-Rev. Med. Chem. 13 (2013) 1487–1500, doi:10.2174/1389557511313100009.

[7] A.S. Kritchenkov, N.A. Bokach, G.L. Starova, V.Y. Kukushkin, A palladium(II) center activates nitrile ligands toward 1,3-dipolar cycloaddition of nitrones substantially more than the corresponding platinum(II) center, Inorg. Chem. 51 (2012) 11971–11979, doi:10.1021/ic301866y.

[8] A.S. Kritchenkov, K.V. Luzyanin, N.A. Bokach, M.L. Kuznetsov, V.V. Gurzhiy, V.Y. Kukushkin, Selective nucleophilic oxygenation of palladium-bound isocyanide ligands: route to imine complexes that serve as efficient catalysts for copper-/phosphine-free sonogashira reactions, Organometallics 32 (2013) 1979–1987, doi:10.1021/om4000665.

[9] L. Brammer, Developments in inorganic crystal engineering, Chem. Soc. Rev. 33 (2004) 476, doi:10.1039/b313412c.

[10] C.-J. Wang, Y.-Y. Wang, J.-Q. Liu, H. Wang, Q.-Z. Shi, S.-M. Peng, Crystal engineering of mixed-ligand frameworks: ligand-directed assembly and structural diversity, Inorganica Chim. Acta. 362 (2009) 543–550, doi:10.1016/j.ica.2008.05.001.

[11] A. Escuer, G. Aromí, Azide as a bridging ligand and magnetic coupler in transition metal clusters, Eur. J. Inorg. Chem. 2006 (2006) 4721–4736, doi:10.1002/ejic.200600552.

[12] D. Braga, F. Grepioni, Intermolecular interactions in nonorganic crystal engineering, Acc. Chem. Res. 33 (2000) 601–608, doi:10.1021/ar990143u.

[13] S.N. Johnson, T.L. Ellington, D.T. Ngo, J.L. Nevarez, N. Sparks, A.L. Rheingold, D.L. Watkins, G.S. Tschumper, Probing non-covalent interactions driving molecular assembly in organo-electronic building blocks, Cryst. Eng. Comm 21 (2019) 3151–3157, doi:10.1039/C9CE00219G.

[14] D. Braga, G.R. Desiraju, J.S. Miller, A.G. Orpen, S.L. Price, Innovation in crystal engineering, Cryst. Eng. Comm 4 (2002) 500–509, doi:10.1039/B207466B.

[15] Bruker, APEX2, SAINT and SADABS, Bruker AXS Inc., Madison, Wisconsin, USA, 2015.

[16] G.M. Sheldrick, SHELXT – integrated space-group and crystal-structure determination, Acta Crystallogr. Sect. A Found. Adv. 71 (2015) 3–8, doi:10.1107/S2053273314026370.

[17] (a) J.J. McKinnon, M.A. Spackman, A.S. Mitchell, Novel tools for visualizing and exploring intermolecular interactions in molecular crystals, Acta Crystallogr. Sect. B Struct. Sci. 60 (2004) 627–668, doi:10.1107/S0108768104020300; (b) Y.-H. Luo, C. Chen, D.-L. Hong, X.-T. He, J.-W. Wang, B.-W. Sun, Thermal-induced dielectric switching with 40K wide hysteresis loop near room temperature, J. Phys. Chem. Lett. 9 (2018) 2158–2163, doi:10.1021/acs.jpclett.8b00597.

[18] J.J. McKinnon, D. Jayatilaka, M.A. Spackman, Towards quantitative analysis of intermolecular interactions with hirshfeld surfaces, Chem. Commun. (2007) 3814–3816, doi:10.1039/B704980C.

[19] M.A. Spackman, D. Jayatilaka, Hirshfeld surface analysis, Cryst. Eng. Comm. 11 (2009) 19–32, doi:10.1039/B818330A.

[20] M.A. Spackman, Molecular electric moments from X-Ray diffraction data, Chem. Rev. 92 (1992) 1769–1797, doi:10.1021/cr00016a005.

[21] M.J. Turner, J.J. McKinnon, S.K. Wolf, D.J. Grimwood, P.R. Spackman, D. Jayatilaka, M.A. Spackman, Crystal Explorer 17, University of Western Australia, Perth, 2017.

[22] M.J. Frisch, G.W. Trucks, H.B. Schlegel, G.E. Scuseria, M.A. Robb, J.R. Cheeseman, G. Scalmani, V. Barone, G.A. Petersson, H. Nakatsuji, X. Li, M. Caricato, A.V. Marenich, J. Bloino, B.G. Janesko, R. Gomperts, B. Mennucci, H.P. Hratchian, J.V. Ortiz, A.F. Izmaylov, J.L. Sonnenberg, D. Williams-Young, F. Ding, F. Lipparini, F. Egidi, J. Goings, B. Peng, A. Petrone, T. Henderson, D. Ranasinghe, V.G. Zakrzewski, J. Gao, N. Rega, G. Zheng, W. Liang, M. Hada, M. Ehara, K. Toyota, R. Fukuda, J. Hasegawa, M. Ishida, T. Nakajima, Y. Honda, O. Kitao, H. Nakai, T. Vreven, K. Throssell, J.A. Montgomery Jr., J.E. Peralta, F. Ogliaro, M.J. Bearpark, J.J. Heyd, E.N. Brothers, K.N. Kudin, V.N. Staroverov, T.A. Keith, R. Kobayashi, J. Normand, K. Raghavachari, A.P. Rendell, J.C. Burant, S.S. Iyengar, J. Tomasi, M. Cossi, J.M. Millam, M. Klene, C. Adamo, R. Cammi, J.W. Ochterski, R.L. Martin, K. Morokuma, O. Farkas, J.B. Foresman, D.J Fox, Gaussian 16, Revision B.01, Gaussian, Inc., Wallingford CT, 2016.

[23] S.F. Boys, F. Bernardi, The calculation of small molecular interactions by the differences of separate total energies. Some procedures with reduced errors, Mol. Phys. 19 (1970) 553–566, doi:10.1080/00268977000101561.

[24] R. Dennington, T. Keith, J. Millam, GaussView, Version 5, Semichem Inc., Shawnee Mission, KS, 2009.

[25] Todd A. Keith, AIMAll (Version 19.10.12), TK Gristmill Software, Overland Park KS, USA, 2019 (aim.tkgristmill.com).

[26] E.D. Glendening, A.E. Reed, J.E. Carpenter, F. Weinhold (Eds.), NBO Version 3.1, Weinhold, 2003.

[27] A.G. Orpen, L. Brammer, F.H. Allen, O. Kennard, D.G. Watson, R. Taylor, Supplement. Tables of bond lengths determined by X-ray and neutron diffraction. Part 2. Organometallic compounds and co-ordination complexes of the d- and f-block metals, J. Chem. Soc. Dalt. Trans. (1989) S1–S83, doi:10.1039/dt98900000s1.

[28] Z. Setifi, F. Setifi, S.W. Ng, A. Oudahmane, M. El-Ghozzi, D. Avignant, Tris(1,10-phenanthroline-κ^2N,N')iron(II) bis(1,1,3,3-tetracyano-2-ethoxypropenide) hemihydrate, Acta Crystallogr. Sect. E Struct. Reports Online 69 (2013) m12–m13, doi:10.1107/S1600536812048611.

[29] Z. Setifi, K.V. Domasevitch, F. Setifi, P. Mach, S.W. Ng, V. Petříček, M. Dušek, Multiple anion…π interactions in tris(1,10-phenanthroline-κ^2N,N')iron(II) bis[1,1,3,3-tetracyano-2-(2-hydroxyethyl)propenide] monohydrate, Acta Crystallogr. Sect. C Cryst. Struct. Commun. 69 (2013) 1351–1356, doi:10.1107/S0108270113027108.

[30] Z. Setifi, F. Setifi, H. Boughzala, A. Beghidja, C. Glidewell, Tris(2,2′-bipyridine)iron(ii) bis(1,1,3,3-tetracyano-2-ethoxypropenide) dihydrate: chiral hydrogen-bonded frameworks interpenetrate in three dimensions, Acta Crystallogr. Sect. C Struct. Chem. 70 (2014) 465–469, doi:10.1107/S2053229614008092.

[31] Z. Setifi, F. Setifi, N. Dege, R. El Ati, C. Glidewell, Redetermination of the crystal structure of Bis(Tri-2-Pyridylamine)Iron(II) Bis(Perchlorate), and a new refinement of the isotypic nickel(II) analogue: treatment of the perchlorate anion disorder, Acta Crystallogr. Sect. E Crystallogr. Commun. 74 (2018) 668–672, doi:10.1107/S2056989018005601.

[32] A. Addala, Z. Setifi, Y. Morimoto, B. Artetxe, T. Matsumoto, J.M. Gutiérrez-Zorrilla, C. Glidewell, Six tris(bipyridyl)iron(ii) complexes with 2-substituted 1,1,3,3-tetracyanopropenide, perchlorate and tetrafluoridoborate anions; order versus disorder, hydrogen bonding and C–N…π interactions, Acta Crystallogr. Sect. E Crystallogr. Commun. 74 (2018) 1717–1726, doi:10.1107/S2056989018015426.

[33] Z. Setifi, F. Setifi, N. Dege, M.H. Al-Douh, C. Glidewell, Bis[tris(pyridin-2-yl)amine]iron(ii) tris(dicyanomethylidene)methanediide, IUCrData 5 (2020) x201278, doi:10.1107/S241431462001278X.

[34] F. Setifi, P. Konieczny, C. Glidewell, M. Arefian, R. Pelka, Z. Setifi, M. Mirzaei, Synthesis, structure, and magnetic properties of a dinuclear antiferromagnetically coupled Iron(II) complex, J. Mol. Struct. 1149 (2017) 149–154, doi:10.1016/j.molstruc.2017.07.085.

[35] Z. Setifi, D. Geiger, C. Jelsch, T. Maris, C. Glidewell, M. Mirzaei, M. Arefian, F. setifi, The first Fe(II) complex bearing end-to-end dicyanamide as a double bridging ligand: crystallography study and hirshfeld surface analysis; completed with a CSD survey, J. Mol. Struct. 1173 (2018) 697–706, doi:10.1016/j.molstruc.2018.07.049.

[36] F. Setifi, Z. Setifi, P. Konieczny, C. Glidewell, S. Benmansour, C.J. Gómez-García, F. Grandjean, G.J. Long, R. Pelka, J. Reedijk, Synthesis, structure and magnetic properties of an unusual oligonuclear Iron(III)-Cobalt(III) compound with oxido-, sulfato- and cyanido-bridging ligands, Polyhedron 157 (2019) 558–566, doi:10.1016/j.poly.2018.10.021.

[37] Z. Setifi, N. Cubillán, C. Glidewell, S.K. Nayak, M. Morales-Toyo, R. Khajavian, F. Setifi, M. Mirzaei, Analysis of supramolecular interactions directing crystal packing of a trans,trans,trans-[Diaquabis(4-Quinolin-3-Yl)-4H-1,2,4-Triazole)Bis(Tricyanomethanide)Iron(II)] complex: a combination of XRD, MEP, NBO, QTAIM, and NCI analyses, J. Mol. Struct. 1228 (2021) 129438, doi:10.1016/j.molstruc.2020.129438.

[38] M.C. Etter, Encoding and decoding hydrogen-bond patterns of organic compounds, Acc. Chem. Res. 23 (1990) 120–126, doi:10.1021/ar00172a005.

[39] M.C. Etter, J.C. MacDonald, J. Bernstein, Graph-set analysis of hydrogen-bond patterns in organic crystals, Acta Crystallogr. Sect. B Struct. Sci. 46 (1990) 256–262, doi:10.1107/S0108768189012929.

[40] J. Bernstein, R.E. Davis, L. Shimoni, N.-L. Chang, Patterns in hydrogen bonding: functionality and graph set analysis in crystals, Angew. Chemie Int. Ed. Eng. 34 (1995) 1555–1573, doi:10.1002/anie.199515551.